5-1996

Relativistic Potential Energy Surfaces of XH2 (X=C, Si, Ge, Sn, and Pb) Molecules: Coupling of 1 A 1 and 3 B 1 States

Nikita Matsunaga
Iowa State University

Shiro Koseki
Mie University

Mark S. Gordon
Iowa State University, mgordon@iastate.edu

Relativistic Potential Energy Surfaces of XH2 (X=C, Si, Ge, Sn, and Pb) Molecules: Coupling of 1 A 1 and 3 B 1 States

Abstract

Potential energy surfaces of the $^1A_1$ and $^3B_1$ states for XH_2 molecules (X=C, Si, Ge, Sn, Pb) are investigated with *ab initio* full valence multiconfigurational self-consistent field wave functions, using effective core potentials. Spin–orbit coupling is also calculated to construct relativistic potential energy surfaces. The relativistic potential energy surfaces are compared with the adiabatic nonrelativistic potentials. Simple one dimensional Landau–Zener transition probabilities are calculated at the minimum energy crossing points of XH_2 molecules to estimate the intersystem crossing probability.

Keywords

Potential energy surfaces, Elemental semiconductors, Germanium, Lead, Ab initio calculations

Disciplines

Chemistry

Comments

The following article appeared in *Journal of Chemical Physics* 104 (1996): 7988, and may be found at 10.1063/1.471515.

Relativistic potential energy surfaces of XH2 (X=C, Si, Ge, Sn, and Pb) molecules: Coupling of 1 A 1 and 3 B 1 states

Nikita Matsunaga, Shiro Koseki, and Mark S. Gordon

Citation: The Journal of Chemical Physics **104**, 7988 (1996); doi: 10.1063/1.471515
View online: http://dx.doi.org/10.1063/1.471515
View Table of Contents: http://scitation.aip.org/content/aip/journal/jcp/104/20?ver=pdfcov
Published by the AIP Publishing

Relativistic potential energy surfaces of XH_2 (X=C, Si, Ge, Sn, and Pb) molecules: Coupling of $^1A_1$ and $^3B_1$ states

Nikita Matsunaga[a)]
Department of Chemistry, Iowa State University, Ames, Iowa 50011-3111

Shiro Koseki
Department of Chemistry, Faculty of Education, Mie University, Tsu, 514, Japan

Mark S. Gordon[b)]
Department of Chemisty, Iowa State University, Ames, Iowa 50011-3111

(Received 4 December 1995; accepted 9 February 1996)

Potential energy surfaces of the $^1A_1$ and $^3B_1$ states for XH_2 molecules (X=C, Si, Ge, Sn, Pb) are investigated with *ab initio* full valence multiconfigurational self-consistent field wave functions, using effective core potentials. Spin–orbit coupling is also calculated to construct relativistic potential energy surfaces. The relativistic potential energy surfaces are compared with the adiabatic nonrelativistic potentials. Simple one dimensional Landau–Zener transition probabilities are calculated at the minimum energy crossing points of XH_2 molecules to estimate the intersystem crossing probability. © *1996 American Institute of Physics.* [S0021-9606(96)03018-7]

INTRODUCTION

Spin–orbit coupling is the major mechanism that connects two adiabatic potential energy surfaces of different spin. This coupling arises due to the interaction between the spin magnetic moment and the orbital motion of an electron around a nucleus. It lifts the degeneracy of a triplet state, for example, into three substates, and with correct symmetries of the spatial and spin parts of the wave function these two states may couple. Spin–orbit coupled states should then give a more realistic view of potential energy surfaces, and it is certainly essential to include spin–orbit coupling in a calculation of potential energy surfaces (PES) of molecules containing heavy elements. For example, one could not possibly obtain even a qualitatively correct dissociation curve of CH_3I[1], due to the spin–orbit splitting of iodine into $^2P_{1/2}$ and $^2P_{3/2}$.

Although the formalism for evaluating spin–orbit coupling matrix elements is available[2] for molecular calculations, there are still a limited number of such calculations, especially as applied to potential energy surfaces[1,3] or chemical reactions[4] of polyatomic molecules.

The effective core potential (ECP) method that projects out core-electron contributions is a powerful way to include heavier elements in calculations on large systems. We have successfully applied ECP's to a number of systems, including main-group[5,6] and transition metal complexes.[7] The ECP method has also been used in the calculations of spin–orbit coupling in order to avoid the rather large computational expense in studying heavy element containing molecules.[8]

The spin–orbit coupling of two different spin states is determined by using a relativistic Breit–Pauli Hamiltonian.[9] Recently, we have utilized the one-electron Breit–Pauli Hamiltonian and systematically deduced the effective nuclear charges of second and third period main group elements using an all-electron basis set.[10] We also reported the effective nuclear charges derived from effective core potentials[11] developed by Stevens *et al.*[12] for second to fifth period alkaline earth and main group elements.

Another method utilizing ECP's to calculate spin–orbit integrals is due to Ermler *et al.*[13] These authors have noted that the differences between the two j-dependent relativistic effective potentials, obtained by fitting the atomic full relativistic Dirac–Hartree–Fock calculations, corresponds to the spin–orbit operator in the core region. Therefore, the gaussian exponents used in the usual ECP integral calculations can be used to define a spin–orbit operator for the core space.

CH_2 is unique among the group IV XH_2 molecules, in that the ground state is a triplet state. The experimental singlet–triplet splitting is in the range 8.5–9.0 kcal/mol.[14] A number of accurate theoretical calculations are also available,[15] in which the calculated singlet–triplet splittings converge close to the experimental values. The lowest singlet state in the remaining group IV A XH_2 species is lower in energy than the lowest triplet states. Several theoretical calculations at various levels of theory have been reported for SiH_2. The most accurate of these place the singlet–triplet splitting at 19–21 kcal/mol.[16]

There are only a handful of theoretical studies[17] dealing with the singlet–triplet splitting and the stationary points on the PES of GeH_2, SnH_2, and PbH_2. The spin–orbit effects are explicitly treated in some of these studies.[17(e),18,19] Electron diffraction derived structures, although they are not dihydrides [XR_2, X=Ge, Sn; R=$CH(SiMe_3)_2$] have also been reported.[20] These are the only experimental XH_2 related structures for heavier group IV A elements in the gas phase.

The energetics, as well as geometries, are affected by large spin–orbit coupling between singlet and triplet states of the heavier group IV A XH_2 compounds. It is certainly interesting to learn how the relativistic PES of XH_2 are different from the adiabatic PES. Here we report potential energy surfaces of XH_2 (X=C, Si, Ge, Sn, and Pb) possessing C_{2v}

[a)]Present address: Department of Chemistry, The Johns Hopkins University, Baltimore, Maryland 21218.
[b)]Author to whom correspondence should be addressed.

 0021-9606/96/104(20)/7988/9/$10.00

symmetry, in which the adiabatic and spin–orbit states of these XH_2 species are compared. The Landau–Zener transition model was also utilized to gain more insight into how transitions between two states might occur.

COMPUTATIONAL APPROACH

The potential energy surfaces of the XH_2 species are prepared with full optimized reaction space (FORS) multiconfiguration self-consistent field (MCSCF or CASSCF) calculations defined by Ruedenberg *et al.*[21] The active space is a full valence space, i.e., six electrons are distributed among six orbitals in the active space. These six orbitals correspond to the two bonding and two antibonding XH bonds, X lone pair and X empty p orbital for a singlet state.

Effective core potentials (ECP), which utilize the averaged relativistic core potentials, of Stevens *et al.*[12] (SBK) are used throughout this paper. Since some of the relativistic effects in the core region, especially contraction of orbitals, are already described with the potentials, geometries obtained with the ECP are expected to be better than those obtained with all-electron basis sets for heavier elements. The lowest singlet ($X\ ^1A_1$) and the lowest triplet ($A\ ^3B_1$) state potential energy surfaces of XH_2 are constructed for a range of bond distances and bond angles, retaining C_{2v} symmetry.

Spin–orbit coupling is calculated by using the one-electron part of the microscopic Breit–Pauli Hamiltonian,[9,10,11]

$$H_{\mathrm{SO}}=\frac{e^2\hbar}{2m^2c^2}\sum_{i,\alpha}\frac{Z_\alpha^{\mathrm{eff}}}{r_{i\alpha}^3}(\mathbf{r}_{i\alpha}\times\mathbf{p}_i)\cdot\mathbf{s}_i, \tag{1}$$

where i runs over all electronic coordinates and α runs over all nuclear centers. Z^{eff} is an adjustable parameter which is determined systematically by adjusting Z^{eff} so that the fine structure splittings of the lowest Π states of diatomic hydrides (XH) are reproduced. Z^{eff} for carbon, silicon, germanium, and tin are 3.90, 168, 1312, and 5500, respectively.[11] Z^{eff} for lead (18200) is chosen to reproduce the fine structure splitting of the Pb atom.

The matrix elements are calculated using the Breit–Pauli spin–orbit operator in Eq. (1), and are placed in a Hamiltonian matrix (4×4 in this case) which is complex. This matrix is diagonalized to obtain the eigenvalues of the four spin-mixed states.

The transition probability is estimated by using a Landau–Zener model[19(b),23] for intersystem crossing. The transition probability P_{LZ} can be given by

$$1-P_{\mathrm{LZ}}=1-e^{-2\delta}, \tag{2}$$

where

$$\delta=\frac{\pi|H_{ij}|^2}{\hbar\nu|\Delta g_{ij}|}, \tag{3}$$

and where H_{ij} is the spin–orbit coupling matrix element between two adiabatic states i and j, ν is the velocity with which the system is passing through the singlet–triplet crossing region, and Δg_{ij} is the difference in the gradients of the two adiabatic states i and j. The transition probability was calculated for a range of kinetic energies.

RESULTS AND DISCUSSION

The stationary points on the adiabatic PES and the relativistic PES of XH_2 are compared with available experiments and relativistic Dirac–Hartree–Fock (DHF) calculations in Table I. The bond lengths of adiabatic XH_2 singlet states calculated with the MCSCF/SBK(d,p) level of theory are 0.04–0.07 Å longer than those for the triplet states. Except for CH_2, the bond angle at which the minimum on the adiabatic PES occurs for singlets is ≈90°, and for triplets the angle is ≈120°. The geometries obtained from the relativistic PES for SiH_2 and GeH_2 do not differ from the adiabatic PES. This is due to the fact that the spin–orbit coupling is smaller than that in the heavier XH_2 species, even though the position of the crossing seam is closer to the triplet minima of SiH_2 and GeH_2 than to the singlet minima. For CH_2 the adiabatic triplet state crosses right at the position of the singlet minimum on the adiabatic surface. Hence a small change in the singlet state geometry results upon mixing of the states by spin–orbit coupling, even though the spin–orbit coupling in CH_2 is the smallest among the XH_2 molecules in the region where the crossing occurs. The MCSCF/SBK(d,p) bond lengths are longer than the corresponding DHF values.

Since there is no two-electron spin-other-orbit coupling term in the DHF calculation, DHF and MCSCF/SBK(d,p) should be in close agreement, except for the fact that our ECP results contain nondynamical correlation through the MCSCF wave functions. Also, the ECP basis set is constructed so as to reproduce the position of the maximum in the atomic radial wavefunctions taken from the DHF calculations.[12] Therefore, relativistic effects, such as inner-shell contractions, are already included in the ECP. The source of any difference in geometry obtained with MCSCF/SBK(d,p) and the DHF calculations should be the nondynamical correlation.

The calculated bond angles are consistently in better agreement with other *ab initio* calculations, than the bond lengths, except for PbH_2, in which both geometrical parameters are not in good agreement. In the present study, the spin–orbit Hamiltonian contains only four elements; therefore, together with the lack of dynamical correlation in the MCSCF wave functions, the discrepancy could come from the omission of higher lying states which may mix with the $^1A_1$ and $^3B_1$ states. For CH_2 to SnH_2, it is more important to consider including dynamical electron correlation, since the effect of spin–orbit coupling on geometries is much smaller than for PbH_2.

Table II shows the calculated vibrational frequencies of adiabatic singlet and triplet states. In general, the triplet states have smaller bending frequencies than the corresponding singlet states, since the triplet bond angles are larger, and the triplet bend potentials are flatter. The stretching frequencies are larger in the triplet, due to the shorter triplet bond

TABLE I. Comparison of MCSCF/SBK(d,p) stationary points of XH_2 adiabatic and spin-mixed potential energy surfaces with Dirac–Hartree–Fock (DHF) relativistic calculations.[a]

	Adiabatic		Relativistic		Experimental or other theoretical calculations	
XH_2	$^1A_1$	$^3B_1$	$^1A_1$	$^3B_1$	$^1A_1$	$^3B_1$
CH_2						
bond length	1.152	1.116	1.150	1.116	1.11,[b]1.11[c]	1.07[b],1.08[c]
bond angle	98.9	129.8	100.1	129.8	102,[b]102.0[c]	134,[b]132.9[c]
SiH_2						
bond length	1.555	1.511	1.555	1.511	1.516[d],1.519[e]	1.484[e]
bond angle	93.4	118.3	93.4	118.3	92.8,[d]92.5[e]	118.5[e]
GeH_2						
bond length	1.620	1.559	1.620	1.559	1.600[f],1.587[g]	1.549,[f]1.534[g]
bond angle	92.3	118.9	92.3	118.9	91.8[f],91.5[g] 92.96[h]	118.9[f],119.8[g]
SnH_2						
bond length	1.793	1.730	1.793	1.734	1.785[g],1.759[h]	1.730[g]
bond angle	92.4	118.4	92.4	116.8	91.1[g],92.55[h]	114.9[g]
PbH_2						
bond length	1.885	1.812	1.880	1.827	1.869[g],1.817[h]	1.865[g]
bond length	90.6	118.6	91.5	115.2	90.5[g],92.29[h]	109.8[g]

[a]Bond lengths are in Å, and bond angles are in deg.
[b]Experimental, see Ref. 14(a).
[c]MRCI, see Ref. 15(c).
[d]Experimental, see Ref. 26.
[e]Second-order CI, see Ref. 16(d).
[f]MRDCI/ECP, see Ref. 17(d).
[g]Spin–orbit CI, see Ref. 17(e).
[h]Dirac–Hartree–Fock, see Ref. 24.

lengths. Among the three vibrational modes the bending mode has the lowest frequencies, and the symmetric stretch is smaller than that of the antisymmetric stretch, except for SnH_2, where the two frequencies are nearly degenerate. This accidental degeneracy allows the two modes to appear as local Sn–H bond stretches.

Potential energy surfaces of XH_2 have been prepared for a range of bond lengths and bond angles. Contour maps of the adiabatic potential energy surfaces of XH_2 are plotted in Fig. 1. In each case, the angle was varied from 60° to 180°. The variation in bond lengths is different for each species. In each figure, the crossing seam between the singlet and triplet is drawn by a bold line. In CH_2 the crossing of singlet and triplet occurs almost exactly at the position of the singlet minimum. As the X atom becomes heavier, the crossing seam moves away from the position of a minimum.

It can be seen from Fig. 1 that the distances between two adjacent contour lines is narrower in the angular direction in all adiabatic triplets. Similarly, the adiabatic singlet has narrower contours along the angular axis, except for SiH_2 and PbH_2. The contour maps of the adiabatic singlet SiH_2 and PbH_2 are almost concentric.

The singlet and triplet surfaces can be coupled through spin–orbit coupling. The nonzero matrix element that contributes to the spin–orbit coupling in a C_{2v} XH_2 molecule is the term arising from the y components of the orbital spin angular momentum operators, respectively (see Appendix for explanation),

$$2^{-1}\alpha^2\langle A_1|l_y|B_1\rangle\langle 1|s_y|3\rangle,$$

where α is the fine structure constant, and $\langle 1|$ and $|3\rangle$ denote singlet and triplet spin functions, respectively. The choice of axes here is such that the atoms in XH_2 are on the $X-Z$ plane in Cartesian space. The rest of the matrix elements are zero in C_{2v} symmetry. The Hamiltonian matrix for mixing these singlet and triplet substates should have the form

$$\begin{array}{c} \\ \langle 0,0| \\ \langle 1,1| \\ \langle 1,0| \\ \langle 1,-1| \end{array} \begin{array}{c} \begin{array}{cccc} |0,0\rangle & |1,1\rangle & |1,0\rangle & |1,-1\rangle \end{array} \\ \begin{pmatrix} {}^1E-\epsilon & x & 0 & x \\ x & {}^3E-\epsilon & 0 & 0 \\ 0 & 0 & {}^3E-\epsilon & 0 \\ x & 0 & 0 & {}^3E-\epsilon \end{pmatrix} \end{array}, \quad (4)$$

TABLE II. Calculated vibrational frequencies[a] of XH_2.

XH_2	Bending	Symm. Str.	Antisymm. Str.
$CH_2(^1A_1)$	1403.2	2766.4	2811.4
$CH_2(^3B_1)$	1139.2	3021.8	3215.6
$SiH_2(^1A_1)$	1005.2	1667.6	1970.9
$SiH_2(^3B_1)$	872.1	2107.5	2167.0
$GeH_2(^1A_1)$	936.5	1822.3	1827.2
$GeH_2(^3B_1)$	819.0	1964.6	2036.4
$SnH_2(^1A_1)$	792.5	1627.3	1627.4
$SnH_2(^3B_1)$	687.1	1747.4	1796.2
$PbH_2(^1A_1)$	721.3	1463.3	1487.7
$PbH_2(^3B_1)$	636.7	1456.8	1606.1

[a]The values are calculated from the MCSCF(6,6)/SBK(d,p) level of theory, and they are in cm^{-1}.

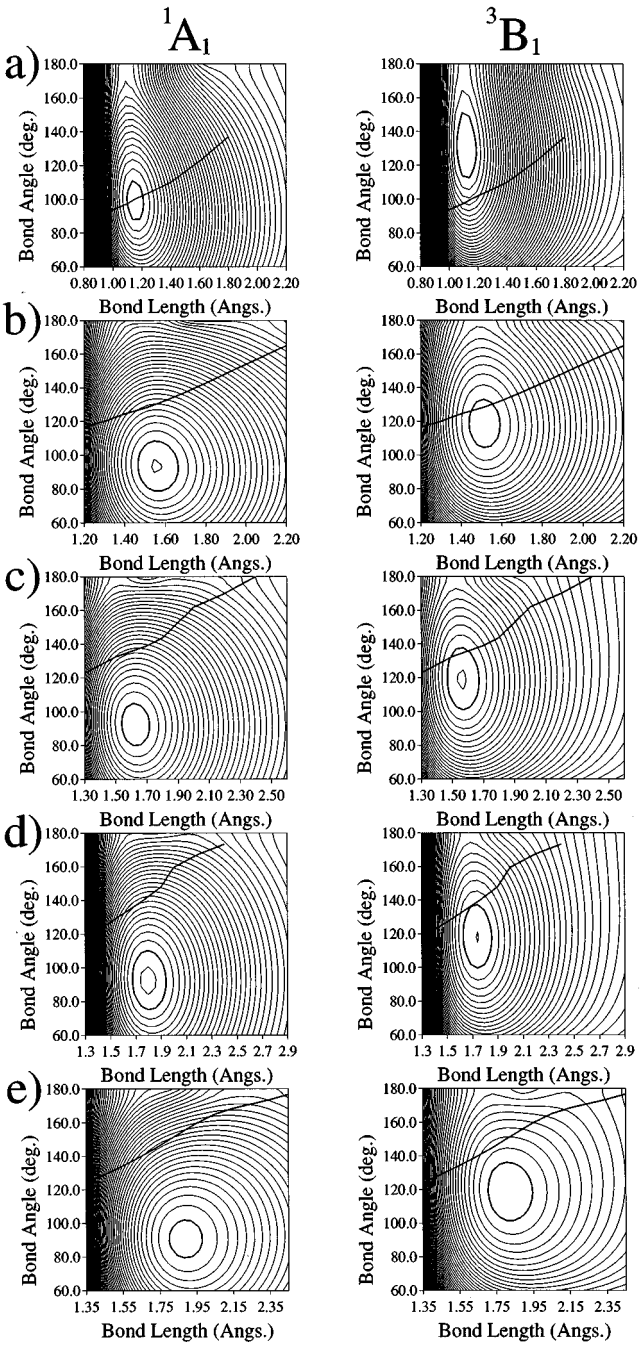

FIG. 1. Contour maps of nonrelativistic potential energy surfaces of XH_2 (X=C, Si, Ge, Sn, Pb). The plots are C_{2v} potential energy surfaces of $^1A_1$ and $^3B_1$ states. Successive contour lines are incremented by 0.005 hartree (1 hartree=627.51 kcal/mol; 1 hartree=2.195×10^5 cm^{-1}). The bold contours of (a) CH_2 indicate -6.555 and -6.570 hartree for singlet and triplet states, respectively. Similarly, (b) SiH_2, -4.880 and -4.855 hartree, (c) GeH_2, -4.855 and -4.815 hartree, (d) SnH_2, -4.445 and -4.410 hartree, and (e) PbH_2, -4.520 and -4.465 hartree. The bold lines indicate crossing seams between singlet and triplet states.

where the bra and ket denote $|S,M_s\rangle$ (S is the total spin angular momentum quantum number and M_s is the z component of the spin quantum number), x denotes the nonzero matrix elements and ^1E and ^3E are the adiabatic singlet and triplet energies, respectively. Due to the coupling of the singlet and a substate of the triplet through the nonzero matrix elements, an avoided crossing between two states out of the four occurs where the adiabatic singlet and triplet states cross. The three spin functions of the triplet can be expressed as $2^{-1/2}(\alpha\beta+\beta\alpha)$, $2^{-1/2}(\alpha\alpha+\beta\beta)$, and $2^{-1/2}(\alpha\alpha-\beta\beta)$. These transform as A_2, B_1, and B_2, respectively.[25(d),17(c)] Hence the overall symmetry of the substates of the triplet are B_2, A_1, and A_2, denoted as $^3B_1(B_2)$, $^3B_1(A_1)$, and $^3B_1(A_2)$. Similarly, the singlet is denoted $^1A_1(A_1)$. Mixing of two substates occurs if the overall symmetry of the two wavefunctions transform according to the same irreducible representation; here $^1A_1(A_1)$ and $^3B_1(A_1)$ mix, and an avoided crossing occurs. The wave functions describing the other two states, $^3B_1(B_2)$ and $^3B_1(A_2)$, can only couple with other high lying states with overall symmetry B_2 and/or A_2. Therefore, these two states are degenerate in the present study, and are described exclusively by triplet character. To lift these degenerate levels, requires the inclusion of higher lying states to form a larger Hamiltonian.

TABLE III. Singlet–triplet splittings of adiabatic and relativistic potential energies of XH_2.[a]

XH_2	Adiabatic $^1A_1-^3B_1$	Relativistic $^1A_1(A_1)-^3B_1(A_1)$
CH_2	10.6	10.6
SiH_2	−16.8	−16.8
GeH_2	−23.9	−24.1
SnH_2	−22.7	−23.7
PbH_2	−33.4	−39.1

[a]The energy of $^1A_1$ with respect to $^3B_1$ in kcal/mol. A positive value indicates that the triplet is energetically more stable. The geometries of each stationary points are used for adiabatic states. For the relativistic splittings, the geometries are optimized by fitting parabolas to the calculated single point energies.

The singlet–triplet energy differences are compared in Table III. This table lists the energy differences for both adiabatic and relativistic singlet and triplet states. The adiabatic singlet–triplet energy gap for the heavier XH_2 becomes larger, except for SnH_2. The latter is actually smaller than that of GeH_2 by 1.2 kcal/mol. The relativistic singlet–triplet splitting does not differ from the adiabatic ones for CH_2, SiH_2, and GeH_2, since the spin–orbit coupling in these molecules is relatively small. In SnH_2 the relativistic singlet–triplet splitting is about 1 kcal/mol larger than the adiabatic value. On the other hand, the splitting becomes almost 6 kcal/mol larger for PbH_2 when the relativistic effects are introduced.

The contour maps for the relativistic XH_2 PES are shown in Fig. 2. Only the $^1A_1(A_1)$ and $^3B_1(A_1)$ states are presented here, as the middle two levels possess exclusively triplet character (vide supra) in the present study. Since there is a coupling between singlet and triplet, one side of the crossing seam on the relativistic PES is predominantly singlet character and the other side of the crossing seam possesses predominantly triplet character. This is especially clear for the species with relatively smaller spin–orbit coupling. For example, the $^1A_1(A_1)$ state of CH_2 in Fig. 2(a)

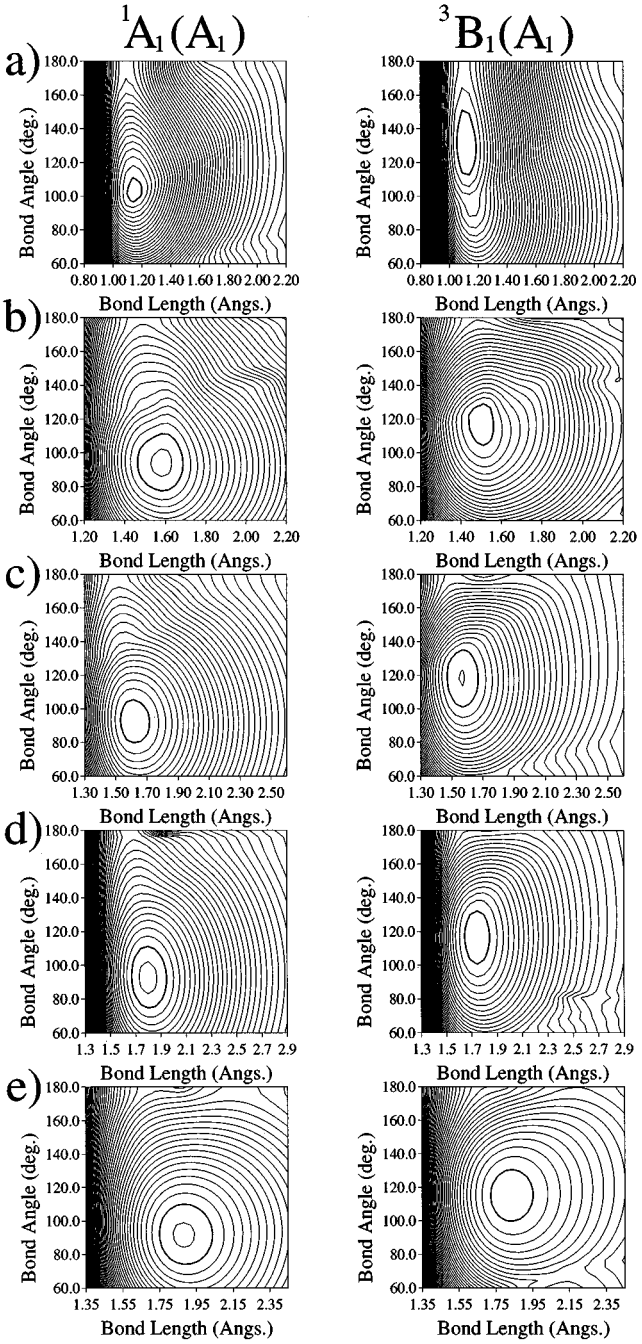

FIG. 2. Contour maps of relativistic potential energy surfaces of XH_2 (X=C, Si, Ge, Sn, Pb). The plots are C_{2v} potential energy surfaces of $^1A_1(A_1)$ and $^3B_1(A_1)$ states. Successive contour lines are incremented by 0.005 hartree (1 hartree=627.51 kcal/mol; 1 hartree=2.195×10^5 cm^{-1}). The bold contours of (a) CH_2 indicate -6.555 and -6.570 hartree for singlet and triplet states, respectively. Similarly, (b) SiH_2, -4.880 and -4.855 hartree, (c) GeH_2, -4.855 and -4.815 hartree, (d) SnH_2, -4.445 and -4.410 hartree, and (e) PbH_2, -4.520 and -4.460 hartree.

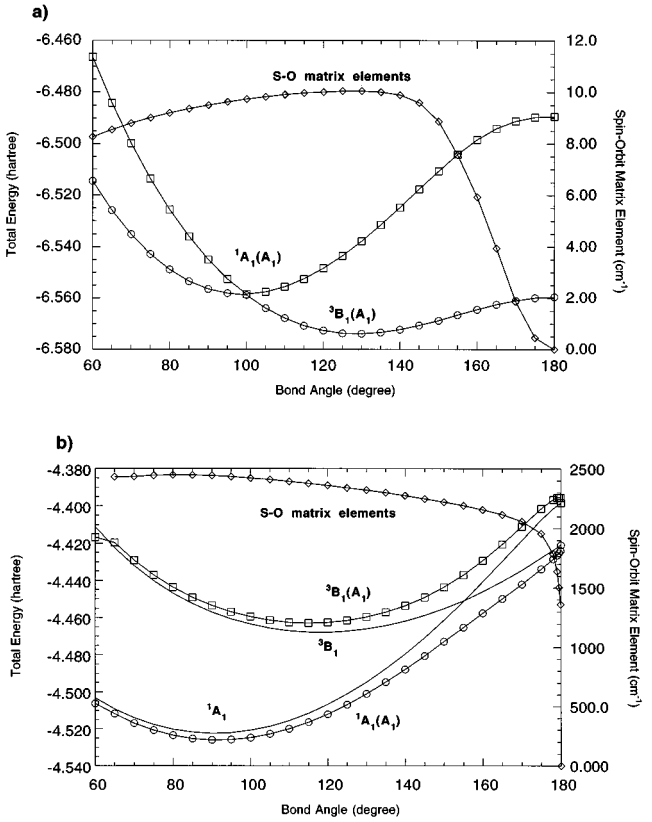

FIG. 3. Cross sectional view of PES of CH_2 and PbH_2. The cross section of (a) relativistic PES of CH_2 at the bond length 1.15 Å is plotted. Also, the spin–orbit coupling matrix elements are shown. (b) PbH_2 PES (bond length 1.885 Å), in which both the adiabatic and relativistic curves, as well as the matrix elements are shown. Note the difference in the scale on the right vertical axis.

shows steeper contours below the crossing seam than the ones shown in Fig. 1(a), in which the lower part of the triplet is connected. Similarly, the $^3B_1(A_1)$ PES in Fig. 2(b) clearly shows adiabatic triplet character above the crossing seam and singlet character below the crossing seam. This becomes less apparent as X becomes heavier and the crossing seam moves to larger HXH angles.

A cross sectional view of the PES is more revealing. Figure 3 shows the cross section of the PES of CH_2 at a fixed bond distance 1.15 Å and the PES of PbH_2 at a fixed bond distance 1.885 Å. Following the top curve (denoted with the squares) of Fig. 3(a) from smaller to larger angle, the curve dramatically changes its character from triplet to singlet. The leading configurations of the wavefunction at a 90° bond angle on the upper curve have triplet character ($2^{-1/2}[\alpha\alpha+\beta\beta]$ combination), accounting for 84.6% of the wave function. The lower curve consists of 90.8% singlet character ($2^{-1/2}[\alpha\beta-\beta\alpha]$). At 110° the upper curve consists of 90.8% singlet character, and the lower curve contains 83.5% triplet character.

Figure 3 also shows spin–orbit coupling matrix elements along the bending coordinates. The spin–orbit coupling for CH_2 becomes larger as angles become larger, and it reaches its maximum value at 135°. Then, it gradually decreases until 140°, then sharply decreases to zero at 180° due to symmetry (see Appendix for more explanation). The spin–orbit coupling trend in PbH_2 is similar to that of CH_2, but the maximum occurs at a smaller angle (80°) and gradually decreases to 175°, then drops steeply to zero at 180°.

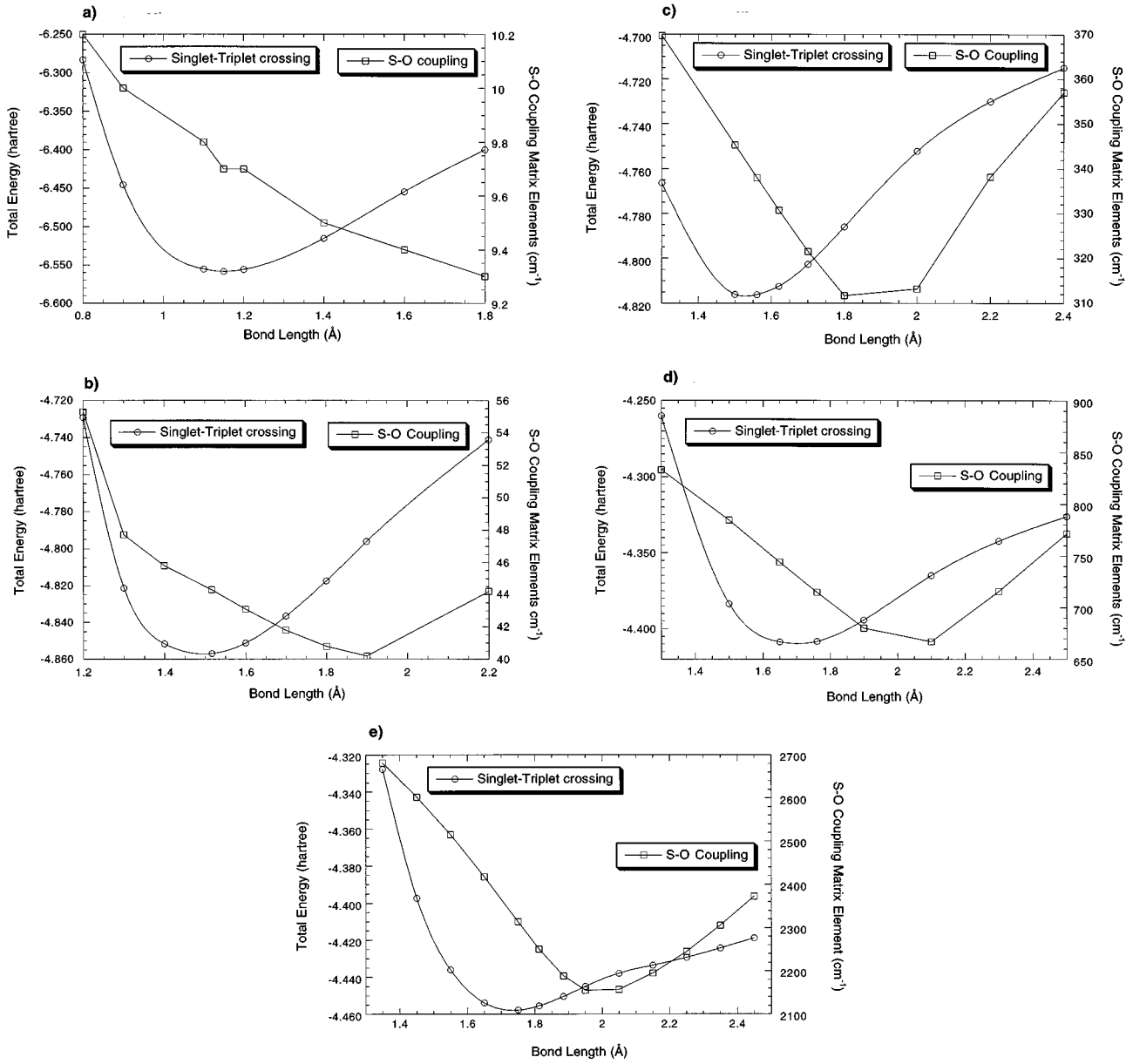

FIG. 4. Energies and spin–orbit coupling matrix elements at crossing seam. Energetics (in hartree) and spin–orbit matrix elements (cm^{-1}) of XH_2 species at crossing seam are plotted against bond lengths. (a) CH_2, (b) SiH_2, (c) GeH_2, (d) SnH_2, and (e) PbH_2.

The minimum energy crossing occurs at 1.15 Å and 100° for CH_2, 1.5 Å and 127.9° for SiH_2, 1.56 Å and 135.7° for GeH_2, 1.65 Å and 134.5° for SnH_2, and 1.75 Å and 146.3° for PbH_2. Figure 4 shows the energetics and the spin–orbit coupling matrix elements along the crossing seam in each XH_2. As can be seen from the figure, the minimum energy crossing occurs at the bond length corresponding to the equilibrium structures on XH_2 upper states ($^1A_1$ for CH_2 and $^3B_1$ for the rest), except for PbH_2, in which the crossing occurs at a bond length that is shorter than that at the stationary point (1.812 Å). The spin–orbit splitting (here we refer to spin–orbit splitting as the splitting between the singlet and triplet states at the crossing points) between $^1A_1(A_1)$ and $^3B_1(A_1)$ along the crossing seam is more or less constant. The spin–orbit couplings in CH_2 and SiH_2 are similar; the coupling is less than 0.5 kcal/mol, with that in SiH_2 slightly larger than CH_2. The splitting in GeH_2 is about 3 kcal/mol. As can be seen from the matrix elements, shown in Fig. 4, the splitting actually becomes smaller until 1.8 Å, then increases again, but the spin–orbit splitting is essentially constant. For SnH_2, the splitting is 6.7–5.5 kcal/mol, and the trend is similar to that found for GeH_2. The splitting for PbH_2 is 24–17 kcal/mol; again there is a decrease in splitting; then it increases.

The transition probability for intersystem crossing using a simple one dimensional Landau–Zener model was calculated for kinetic energies ranging from 0 to 2.0 eV. Figure 5 shows the transition probabilities calculated at the minimum energy crossing points for XH_2 species. A probability of unity means that the transition would take place as the molecule traverses the crossing point in one pass. As can be seen

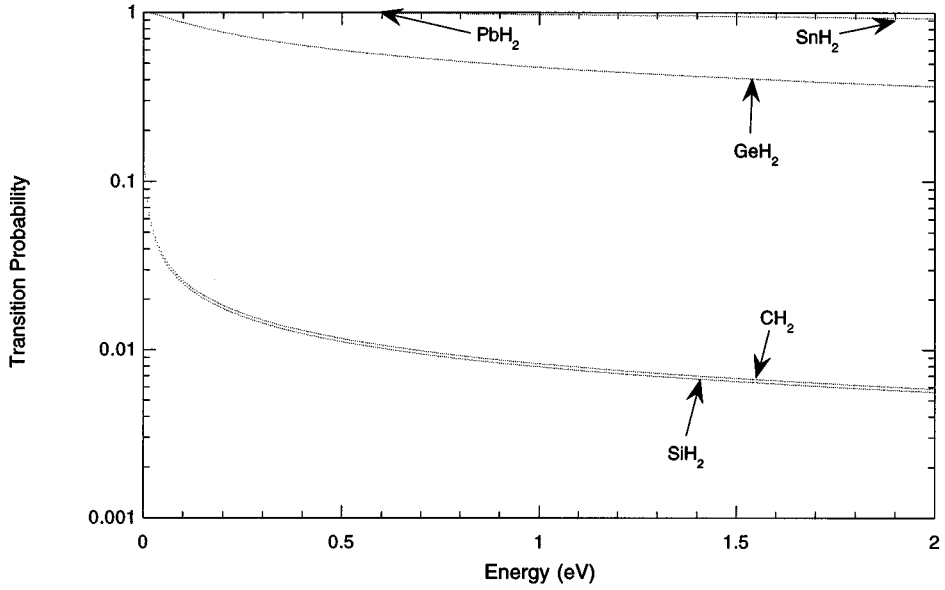

FIG. 5. Transition probability of XH_2. Transition probability, using the Landau–Zener model, is calculated at the minimum energy crossing point of the C_{2v} potential energy surfaces as a function of kinetic energy (eV), at which a molecule crosses the intersection in a single pass.

from the figure, CH_2 and SiH_2 have a similar transition profile, in which the transition would take place only in a small kinetic energy region. On the other hand, transition is accessible at any kinetic energy in SnH_2 and PbH_2. Strong spin–orbit coupling for a given kinetic energy and a larger mass in SnH_2 and PbH_2 for given kinetic energy *both* contribute to larger intersystem crossing probability. GeH_2 is an intermediate case for which the transition is accessible in a range of kinetic energies.

The bending frequency of $^3B_1$ CH_2 (1139.2 cm^{-1}) roughly corresponds to 0.07 eV. This translates to a transition probability 0.03. Hence, even in the small spin–orbit coupling limit and large bending frequency limit, as in CH_2, a molecule that crosses the intersection in a single pass, would have a 3% intersystem crossing probability.

CONCLUSIONS

The PES of adiabatic and spin–orbit coupled states of XH_2 (X=C, Si, Ge, Sn, and Pb) species have been compared. The geometries of SiH_2 and GeH_2 at the stationary points on the relativistic PES do not differ from the ones on the adiabatic PES due to small spin–orbit coupling. For CH_2, the singlet–triplet crossing seam lies at the position of the singlet minimum; therefore a small change in geometry is observed. The triplet state of SnH_2 is shifted 0.004 Å in bond length and 1.6° in bond angle on the relativistic PES. Due to strong spin–orbit coupling, the geometries of PbH_2 are shifted 0.005 Å and 1° for singlet and 0.015 Å and 3.4° for triplet.

Due to the coupling of singlet and triplet, the relativistic PES appears as predominantly singlet on one side and predominantly triplet on the other side of the crossing seam. If the coupling is strong, as found in PbH_2, the relativistic PES can differ dramatically from the adiabatic PES.

The spin–orbit coupling affects the singlet–triplet splitting only for SnH_2 (by 1 kcal/mol) and 6 kcal/mol for PbH_2. The splittings in CH_2, SiH_2, and GeH_2 are not affected.

The bond length at which the minimum energy crossing occurs is closer to that of the higher of the two energy states (singlet for CH_2 and triplet for the rest). The energy separation between the spin–orbit coupled states is less than 1 kcal/mol for CH_2 and SiH_2, and for GeH_2 it is about 3 kcal/mol. For SnH_2, the energy separation is 5.5–6.7 kcal/mol, and for PbH_2 it is 17–24 kcal/mol.

Transition probabilities for intersystem crossing are calculated using the Landau–Zener model. The intersystem crossing occurs only for relatively small kinetic energy regions in CH_2 and SiH_2. However, for SnH_2 and PbH_2 a transition is readily accessible at any kinetic energy due to the strong spin–orbit coupling and larger mass. GeH_2 is an intermediate case, for which the transition is accessible in a range of kinetic energies.

ACKNOWLEDGMENTS

This work was supported by grants from Air Force Office of Scientific Research (F49620-95-1-0077) and the National Science Foundation (CHE-93-13717). The authors wish to acknowledge helpful discussions with Dr. Tetsuya Taketsugu, Dr. Satoshi Yabushita, and Dr. Michael W. Schmidt during the course of this project. The authors also wish to acknowledge Dr. Greg Atchity for providing us with a contouring program CNTOUR in ALIS system of programs.

APPENDIX

The spin–orbit matrix element between $^1A_1$ and $^3B_1$ states in C_{2v} symmetry can be expressed as[25]

$$\langle {}^1A_1|H_{\mathrm{SO}}|{}^3B_1\rangle=\langle {}^1A_1|l\cdot s|{}^3B_1\rangle. \tag{A1}$$

It is assumed that both sides of Eq. (A1) are multiplied by $\alpha^2/2$ where α is the fine structure constant, $e\hbar^{1/2}/mc$. By utilizing ladder operators, $l\cdot s$ can be written as

$$l\cdot s=l_z s_z+\frac{1}{2}\,l^+ s^-+\frac{1}{2}\,l^- s^+, \tag{A2}$$

where l_z is the z-component of the orbital angular momentum operator and s_z is the z-component of the spin angular momentum operator. l^+ and l^- are the raising and lowering operators for orbital angular momentum, respectively, and are defined as

$$\begin{aligned} l^+&\equiv l_x+il_y,\\ l^-&\equiv l_x-il_y. \end{aligned} \tag{A3}$$

Similarly, s^+ and s^- are the raising and lowering spin angular momentum operators, respectively,

$$\begin{aligned} s^+&\equiv s_x+is_y,\\ s^-&\equiv s_x-is_y. \end{aligned} \tag{A4}$$

Substituting Eq. (A2) into Eq. (A1) gives

$$\begin{aligned} \langle {}^1A_1|l\cdot s|{}^3B_1\rangle=&\langle A_1|l_z|B_1\rangle\langle 1|s_z|3\rangle+\frac{1}{2}\,\langle A_1|l^+|B_1\rangle\\ &\times\langle 1|s^-|3\rangle+\frac{1}{2}\,\langle A_1|l^-|B_1\rangle\langle 1|s^+|3\rangle. \end{aligned} \tag{A5}$$

Here $|1\rangle$ and $|3\rangle$ denote appropriate singlet and triplet spin functions. The three triplet spin functions are $2^{-1/2}(\alpha\beta+\beta\alpha)$, $2^{-1/2}(\alpha\alpha+\beta\beta)$, and $2^{-1/2}(\alpha\alpha-\beta\beta)$, and these transform as A_2, B_1, and B_2 irreducible representations in C_{2v} symmetry.[25] The l_x, l_y, and l_z operators transform as B_2, B_1, and A_2 irreducible representations, respectively. A spin operator transforms as a rotation; therefore, the s_x, s_y, and s_z operators transform as B_2, B_1, and A_2, respectively, in C_{2v} symmetry. Substituting Eqs. (A3) and (A4) into Eq. (A5), and using the fact that the spin–orbit Hamiltonian is totally symmetric, the nonzero spin–orbit matrix element between ${}^1A_1$ and ${}^3B_1$ is

$$\begin{aligned} \langle {}^1A_1|l\cdot s|{}^3B_1\rangle=&\langle A_1|l_y|B_1\rangle\langle 1|s_y|3\rangle\\ &\neq 0 \text{ for triplet spin function}\\ &2^{-1/2}(\alpha\alpha+\beta\beta). \end{aligned}$$

The only nonzero spin–orbit matrix element between ${}^1A_1$ and ${}^3B_1$ states arises from the term containing the l_y angular momentum operator and the s_y spin operator for the $\alpha\alpha+\beta\beta$ triplet spin functions.

Similar group theoretical arguments can be applied to deduce the matrix element connecting ${}^1\Delta_g$ and ${}^3\Sigma_g^-$ states of $D_{\infty h}$ XH_2 molecules is zero.

[1] (a) S. Yabushita and K. Morokuma, Chem. Phys. Lett. **153**, 517 (1988); (b) Y. Amatatsu, K. Morokuma, and S. Yabushita, J. Chem. Phys. **94**, 4858 (1991).

[2] (a) H. F. King and T. R. Furlani, J. Comput. Chem. **9**, 771 (1988); (b) T. R. Furlani, Ph.D. dissertation, State University of New York at Buffalo, Buffalo, 1984; (c) P. Abegg, W. Mol. Phys. **30**, 579 (1975); (d) L. E. McMurchie, and E. R. Davidson, J. Comput. Phys. **26**, 218 (1976).

[3] (a) T. R. Furlani and H. F. King, J. Chem. Phys. **82**, 5577 (1985); (b) R. A. Caldwell, L. Carlacci, C. E. Doubleday, T. R. Furlani, H. F. King, and J. W. McIver, J. Am. Chem. Soc. **110**, 6901 (1988).

[4] (a) M. R. Manaa and D. R. Yarkony, J. Chem. Phys. **95**, 1808 (1991); (b) K. A. Nguyen, M. S. Gordon, J. A. Montgomery, H. H. Michels, and D. R. Yarkony, *ibid*. **98**, 3845 (1993).

[5] (a) N. Matsunaga, T. R. Cundari, M. W. Schmidt, and M. S. Gordon, Theor. Chim. Acta **83**, 57 (1992); (b) N. Matsunaga, M. S. Gordon, J. Am. Chem. Soc. **116**, 11 407 (1994).

[6] (a) M. S. Gordon, K. A. Nugyen, and M. T. Carrol, Polyhedron **10**, 1247 (1991); (b) K. A. Nugyen, M. T. Carroll, and M. S. Gordon, J. Am. Chem. Soc. **113**, 7924 (1991).

[7] (a) T. R. Cundari and M. S. Gordon, J. Am. Chem. Soc. **114**, 539 (1992); (b) Organomet. **11**, 55 (1992); (c) T. R. Cundari, J. Am. Chem. Soc. **114**, 7889 (1992).

[8] (a) J. S. Cohen, W. R. Wadt, and P. J. Hay, J. Chem. Phys. **71**, 2955 (1979); (b) W. R. Wadt, Chem. Phys. Lett. **89**, 245 (1982).

[9] (a) S. R. Langhoff and C. W. Kern, in *Modern Theoretical Chemistry*, edited by H. F. Schaefer Vol. 3, Chap. 10, p. 381; (b) D. R. Yarkony, Int. Rev. Phys. Chem. **11**, 195 (1992).

[10] S. Koseki, M. W. Schmidt, and M. S. Gordon, J. Phys. Chem. **96**, 10 768 (1992).

[11] S. Koseki, M. S. Gordon, M. W. Schmidt, and N. Matsunaga, J. Phys. Chem. **99**, 12 764 (1995).

[12] (a) W. J. Stevens, H. Basch, and M. Krauss, J. Chem. Phys. **81**, 6026 (1984); (b) W. J. Stevens, H. Basch, M. Krauss, and P. Jaisen, Can. J. Chem. **70**, 612 (1992); (c) T. R. Cundari and W. J. Stevens, J. Chem. Phys. **98**, 5555 (1993).

[13] W. C. Ermler, Y. S. Lee, P. A. Christiansen, and K. S. Pitzer, Chem. Phys. Lett. **81**, 70 (1981).

[14] (a) A. R. W. McKellar, P. R. Bunker, T. J. Sears, K. M. Evenson, R. J. Saykally, and S. R. Langhoff, J. Chem. Phys. **79**, 5251 (1983); (b) D. G. Leopold, K. K. Murray, A. E. Stevens Miller, and W. C. Lineberger, *ibid.* **83**, 4849 (1985).

[15] (a) X. Li, P. Piecuch, and J. Paldus, Chem. Phys. Lett. **224**, 267 (1994); (b) P. J. Reynolds, M. Dupuis, and W. A. Lester, Jr., J. Chem. Phys. **82**, 1983 (1985); (c) C. W. Bauschlicher, S. R. Langhoff, and P. R. Taylor, *ibid*. **87**, 387 (1987).

[16] (a) M. E. Colvin, R. S. Grev, and H. F. Schaefer, Chem. Phys. Lett. **99**, 399 (1983); (b) J. E. Rice and N. C. Handy, *ibid*. **107**, 365 (1984); (c) M. S. Gordon, *ibid*. **114**, 348 (1985); (d) K. Balasubramanian, and A. D. McLean, J. Chem. Phys. **85**, 5117 (1986); (e) M. S. Gordon, D. R. Gano, J. S. Binkley, and M. J. Frisch, J. Am. Chem. Soc. **108**, 2191 (1986); (f) S. Koseki and M. S. Gordon, J. Mol. Spectrosc. **123**, 392 (1987); (g) A. Selmani and D. R. Salahub, J. Chem. Phys. **89**, 1529 (1988).

[17] (a) G. Olbrich, Chem. Phys. Lett. **73**, 110 (1980); (b) J.-C. Barthelat, B. S. Roch, G. Trinquier, and J. Satge, J. Am. Chem. Soc. **102**, 4080 (1980); (c) R. A. Philips, R. J. Buenker, R. Beardsworth, P. R. Bunker, P. Jensen, and W. P. Kraemer, Chem. Phys. Lett. **118**, 60 (1985); (d) L. G. M. Pettersson and P. E. M. Siegbahn, Chem. Phys. **105**, 355 (1986); (e) K. J. Balasubramanian, *ibid.* **89**, 5731 (1988); (f) see Ref. 16(e).

[18] (a) K. Balasubramanian, Chem. Phys. Lett. **127**, 585 (1986); (b) see Ref. 17(e).

[19] (a) See Ref. 17(e); (b) P. Schwerdtfeger, H. Silberbach, and B. Miehlich, J. Chem. Phys. **90**, 762 (1989).

[20] T. Fjeldberg, A. Haaland, B. E. R. Schilling, M. F. Lappert, and A. J. Thorne, J. Chem. Soc. Dalton Trans. **1986**, 1551.

[21] K. Ruedenberg, M. W. Schmidt, M. M. Gilbert, and S. T. Elbert, Chem. Phys. **71**, 41, 51, 65 (1982).

[22] (a) M. W. Schmidt, K. K. Baldridge, J. A. Boatz, S. T. Elbert, M. S.

Gordon, J. H. Jensen, S. Koseki, N. Matsunaga, K. A. Nugyen, S. Su, T. L. Windus, M. Dupuis, and J. A. Montgomery Jr., J. Comput. Chem. **14**, 1347 (1993); (b) contact Mike Schmidt at mike@si.fi.ameslab.gov concerning this program.
[23] H. Nakamura, J. Chem. Phys. **87**, 4031 (1987).
[24] K. G. Dyall, J. Chem. Phys. **96**, 1210 (1992).
[25] (a) J. W. Sidman, J. Chem. Phys. **29**, 644 (1958); (b) W. R. Hall and H. F. Hameka, *ibid.* **58**, 226 (1973); (c) S. R. Langhoff, *ibid.* **61**, 3881 (1974); (d) R. M. Pitzer and N. W. Winter, J. Phys. Chem. **92**, 3061 (1988).
[26] I. Dubois, Can. J. Phys. **46**, 2485 (1968).